

Enhanced field ionization/desorption on branched silicon nanowires: applications in gas ionization detection

R. Banan-Sadeghian* and M. Saif Islam

Dept. of Electrical and Computer Engineering, University of California – Davis
One Shields Avenue, Kemper Hall, Davis, CA, 95616

ABSTRACT

We demonstrate anomalous gaseous field ionization and field desorption on branching intrinsic silicon nanowires grown by a two-step VLS technique. Field ionization and desorption I - V curves of argon, nitrogen, helium, and ammonia, were recorded individually within a wide pressure range (10^{-7} to 10 Torr). Field ionization initiated at sub volt was followed by field desorption at about 7 – 38 V (applied field of $\sim 7 \times 10^2$ to 3.8×10^3 V/cm). Such voltages are three orders of magnitude smaller than the applied voltages required to generate field ionization on sharp metallic tips having the same tip curvature. The measured I - V curves were pressure dependent. Low voltage field ionization and desorption phenomena were attributed to the combination effects of geometrical field enhancement on the apex of nanoscale silicon branches, field penetration, increased tunneling critical distance, band gap widening due to quantum confinement, and the surface states formed by the catalyst. The results presented herein suggest that gold terminated branching silicon nanowires could be strong candidates in building low power gas ionization sensors useful in highly selective detection of gases with low adsorption energies.

Keywords: field ionization, field desorption, branching silicon nanowires, gas ionization sensing

1. INTRODUCTION

Of late, silicon nanowires have become subject of intense research due to their unique physical properties and potential integration with standard CMOS electronic and photonic devices. Namely, various electrical characteristics of nanowires grown by chemical-vapor-deposition (CVD) have been determined¹⁻⁴. However, to the best of our knowledge, there has been no report on ion generation phenomena such as field ionization, desorption or evaporation of molecules subjected to high electric fields at the apex of these nanowires. This paper reports occurrence of field ionization and desorption actions at anomalously low potentials on branching silicon nanowires grown by a two-step vapor-liquid-solid (VLS) technique using gold as the catalyst. Branching nanowires of silicon have been previously synthesized with⁵ or without⁶ re-seeding the primary nanowire array. Because of their high surface-to-volume ratio, these nanostructures offer potential applications in solar energy harvesting and conversion⁷, molecular scale electron devices, and chemical sensors. Our observations on field ionization of gaseous species using branching nanowires at small bias voltages can potentially offer opportunities for applications such as, mass spectrum analysis, scanning helium-ion microscopy, and miniaturized gas ionization detection^{8,9}, making branched silicon nanowires a strong contender for micromachined field-ionization sources. Although recent developments in fabrication of dense nanostructures with ultra-sharp tips offered promises for field-ionization of gas molecules at reduced bias voltages, for their accurate fingerprinting, the operating voltages are still in the order of a few hundred volts.

In this work, however, measurable field-ion currents of nitrogen, argon and helium were recorded at sub-10 V, that is, three orders of magnitude smaller than the voltages recorded using sharp metallic specimens¹⁰. We believe such enhanced ionization phenomena cannot be merely due to the large field amplification factor of sharp silicon branches terminated with gold nanoparticles. Positive field penetration causes upward band bending at the surface of exposed silicon that contains gold-induced surface states at the vicinity of the catalyst. Band bending allows the valence electron to tunnel into the degenerate states of the valence band, or into the surface states, at considerably reduced imaging fields¹¹⁻¹⁵. Depending on the bias voltage (1–100V), various pressure-dependent regimes of discharge were observed.

* rbsadegh@ucdavis.edu; phone 1 530 754-2257; fax 1 530 752-8428; www.ece.ucdavis.edu/~rbsadegh/

2. EXPERIMENTAL

2.1 Synthesis of branching and non-branching Si nanowire arrays

Lightly doped branching silicon nanowires were grown by a two-step VLS approach similar to Doerk et al.'s work⁶, using SiH_4 instead of SiCl_4 as the precursor. $2\text{cm} \times 2\text{cm}$ dices of p -type Si (111) ($\rho < 0.005 \Omega\text{-cm}$) were prepared and degreased by sonicating in acetone, isopropanol, and methanol, and then rinsed with deionized water. The samples were next immersed in a 2% HF (v/v) for 60 sec to remove the native oxide, rinsed with deionized water, and dried under nitrogen stream. In order to secure ohmic connection to the nanowires, the backside of the dices was sputter-coated with a relatively thick (200 nm) aluminum layer. Finally, a 3 nm thick film of gold was evaporated on the polished side of the dices with a rate of 3 \AA min^{-1} . After gold deposition, the substrates were transferred into a quartz-tube CVD reactor and heated at 610°C for 20 minutes in an environment of 10 Torr H_2 in order to form Au-Si alloy and then dewet the film creating an array of alloy droplets. Figure 1 shows a schematic of the nanowire synthesis steps in sequence.

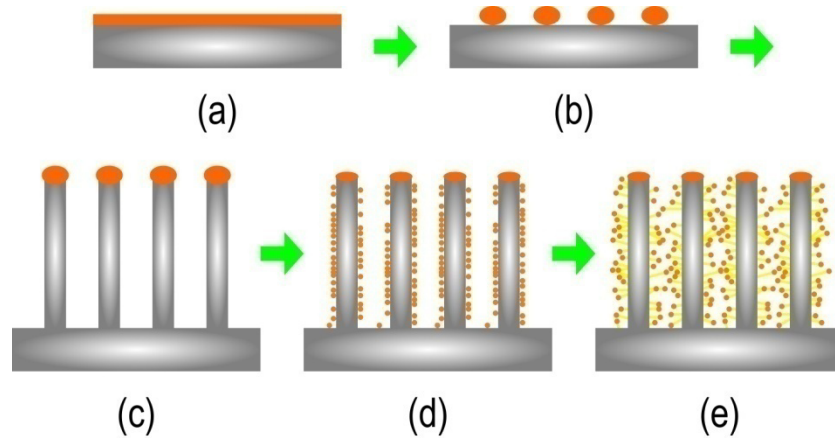


Figure 1. A schematic illustration of the process steps used to grow branching silicon nanowires: (a) Electron-beam deposition of a 3nm thick gold layer. (b) Annealing at 610°C to form Au-Si alloy and then Au-Si liquid droplets above the eutectic point. (c) Growth of primary nanowire trunks at 680°C . (d) Downward migration of Au-Si nanoparticles from the tip during an intermediate annealing step in HCl. (e) Simultaneous growth of nanowire branches from the migrated Au-Si nanoparticles and the primary nanowires from catalyst remaining at the tips.

Primary nanowires were then grown at 680°C by introducing SiH_4 with a flow rate of 15 sccm for one hour. They attained an average length of $\sim 15 \mu\text{m}$ and an average diameter of $\sim 400 \text{ nm}$. After growing the primary trunks, an intermediate annealing step was performed by first removing the SiH_4 source and then ramping down the temperature from 680°C to 580°C in 15 minutes. During the ramp down, HCl was introduced to the chamber with a flow rate of 15 sccm to inhibit further growth of nanowires and cause downstream migration of the Au-Si eutectic in form of nanoparticles (Figure 1d). Growth of the forest of branches was initiated by removing the HCl source and then reintroducing SiH_4 with the same rate as for the primary growth, but this time for 5 minutes at 580°C . Finally, the flow of SiH_4 was stopped and the reactor was cooled down to room temperature. Smooth silicon nanowires were synthesized employing the same procedure, except the secondary growth step was not carried out. SEM micrographs of the as-grown arrays of branching and non-branching nanowires are presented in Figure 2. It can be seen that the growth of primary nanowires has been continued during the secondary growth step because the catalyst was still present at the tips. However, discernable is a change in the growth direction which can be attributed to the gradual reduction of the reactor temperature during this step.

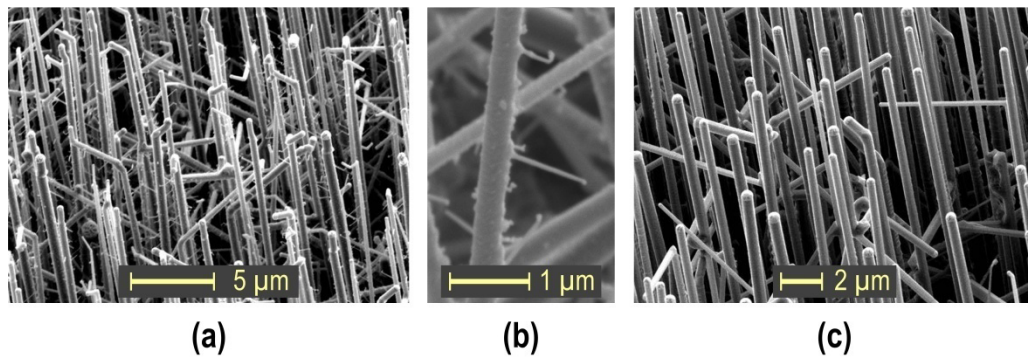


Figure 2. SEM micrographs of the as-grown Si nanowires: (a) and (b) Branching nanowires grown by reintroducing SiH_4 after the intermediate annealing step. (c) non-branching nanowires.

2.2 Fabrication of the ionization cells

Two types of ionization cell (IC) were fabricated using *branching* and *non-branching* (smooth) silicon nanowires at the anode electrode. These devices had otherwise identical features. The measurements reported here were carried out on one device instance carrying smooth silicon nanowires, and two instances having branching nanowires, henceforth referred to as IC.**smooth**, IC.**branched#1**, and IC.**branched#2**, respectively. Figure 3 represents a three dimensional schematic view of an IC. A circular slab of aluminum as the counter electrode (cathode), was mounted over the substrate. Intermittent pieces of highly-insulating polypropylene film were used as spacers between the electrodes, creating a gap spacing of ca. $100\ \mu\text{m}$. As illustrated in Figure 3, flow of gas into the ionization zone was possible through the spacer voids. Finally, ohmic connections were established to both of the electrodes using silver epoxy.

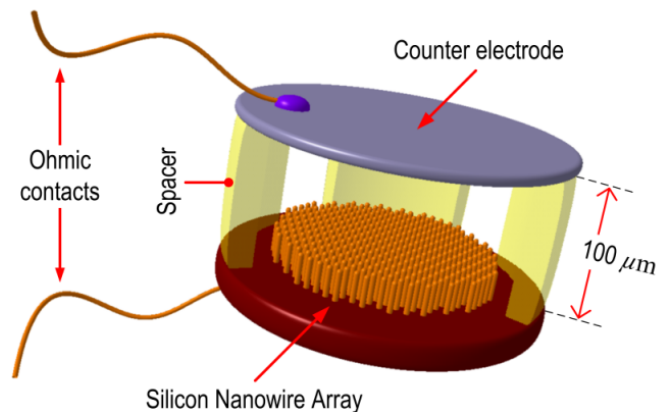


Figure 3. A 3D schematic view of an IC showing the generic silicon nanowire array at the anode. Note the dimensions are not in scale, in particular the inter-electrode spacing is oversized.

2.3 Measurement setup and agenda

Current-Voltage (I - V) measurements were carried out inside a custom built vacuum chamber that could accommodate test gases and gas admixtures within a total pressure range of 10^{-7} to 760 Torr. The chamber was equipped with roughing and turbo pumps, a manual gate valve, multiple precision MFCs capable of regulating flow rates down to sccm scale, and electrical feedthroughs with Triax to BNC adaptors. A photograph of the chamber is presented in Figure 4.

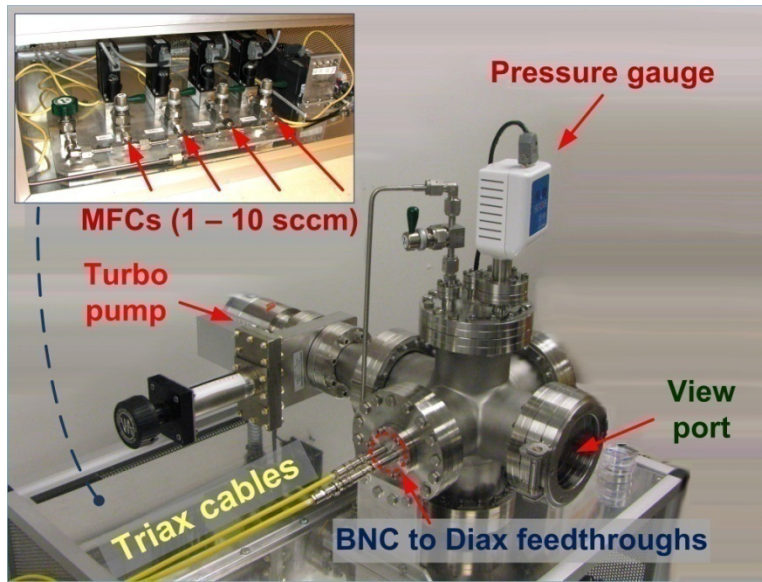


Figure 4. PC-PLC based custom-made vacuum chamber designed to meet our gas ionization sensing requirements.

Prior to each experiment, the chamber was purged with anhydrous nitrogen for 10 minutes to ensure removal of any water molecules and then pumped down to a base pressure of $\sim 10^{-7}$ Torr. Test gases were resealed from the MFCs until equilibrium pressure was reached. Stepwise voltage sweep was conducted in differential mode in room temperature using two source measure units (SMUs) of an HP4155 semiconductor parameter analyzer connected in series. In this fashion, the currents to either electrode were recorded separately. In order to minimize capacitive leakage currents, guarded Triax cables were used.

3. RESULTS AND DISCUSSION

Measurable field ionization was detected only on branched silicon nanowires. Using IC.**branched**#1 first, the anode and cathode currents were recorder in nitrogen at chamber base pressure ($P = 3 \times 10^{-7}$ Torr). Figures 5a and 5b show the electrode currents in linear and log-log scales respectively. As shown in Figure 5a, below $V \approx 24V$ the source of conduction is merely electron thermionic emission from the flat cathode, as the cathode current varies little with voltage. Because of a highly nonlinear field distribution at the anode, there is a slight increase with voltage discernable in the anode current until field ionization takes effect and the current increases over-exponentially. The slight increase of the anode current was also observable in IC.**smooth** but to a milder degree and within a wider voltage range, however, no field ionization was detected. Figures 6a and 6b show the $I-V$ curves of nitrogen measured by IC.**smooth** and IC.**branched**#1 respectively. At ultimate low pressures, the conduction mechanism in IC.**smooth** appears to be similar to that of uniform field conditions, where at low voltages current flows due to already existing electron-ion pairs generated by cosmic radiation. In this regime, the $I-V$ relationship exhibits an ohmic behavior and the discharge current density is given by

$$J_{\Omega} = e(n_e \mu_e + n_i \mu_i) \bar{E}, \quad (1)$$

where e is the electron charge, \bar{E} is the effective uniform field along the gap, n_e and n_i are the electron and ion concentrations, and μ_e and μ_i are the mobilities, assuming to be constant at low fields. Equation (1) remains valid as long as there is no space charge to affect \bar{E} . As the field increases, the discharge current tends to saturate because all of the generated carriers arrive at the electrodes. The saturated current density is therefore limited by the rate of carrier generation and is given by

$$J_{sat} = de \frac{dn}{dt}, \quad (2)$$

where d is the gap spacing and dn/dt is the carrier generation rate. At intermediate pressures ($10^{-5} \leq P \leq 10^{-4}$ Torr), the discharge current shows a logarithmic dependence on pressure because carrier generation in the gap gently becomes limited by the diffusion of gas molecules. Note that in general, diffusivity, D , exponentially increases with the reduced field (E/P), or decreases with pressure if a constant field is stipulated. Diffusion of gas into the gap spacing becomes the limiting factor at high pressures, as a result, the discharge current drops for $P \geq 10^{-4}$. The inset at Figure 6a shows the curves of discharge current versus pressure at three bias voltages.

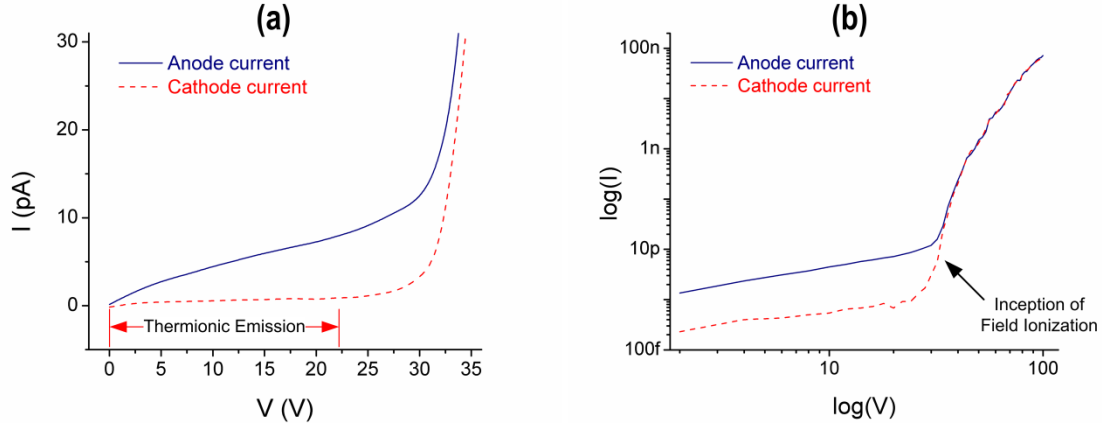


Figure 5. Current-Voltage curves recorded from either electrodes of IC.branched#1 with the nanowires configured at the anode: (a) linear and (b) log-log scale. The curves were obtained in nitrogen ($P = 3 \times 10^{-7}$ Torr).

In IC.branched#2, ohmic conduction ceases at lower voltages due to field ionization. This is clearly discernable in the full logarithmic I - V plots of Figure 6b for $1 \leq V \leq 7$ V, as the slope of the curves in this range are slightly greater than unity. At low fields close to the threshold, the gas distribution close to the branch tips is in equilibrium. The ion current in this case is proportional to the number of particles near the tips and rigorously depends on the field strength (is field-limited). Field-limited ion current emitted from a single hemispherical tip is approximately given by

$$I_{FL} = 2\pi r_w^2 e x_c c_t \nu_e \Gamma, \quad (3)$$

where r_w is the tip curvature, c_t is the equilibrium gas concentration near the tip, ν_e is the orbital frequency of the tunneling electron, Γ is the ionization probability, and x_c is the critical distance between the tip and the ionizing gas molecule below which electron tunneling cannot occur¹⁶. x_c is about 4 – 5 Å for metallic tips. At a constant field and gas concentration, I_{FL} is solely a strong function of the molecular ionization potential, U_i , and polarizability, α , through x_c and Γ . Such dependence can be employed to fingerprinting the unknown gas molecule since these quantities are unique to each molecule type. On the contrary, no tangible difference was observed in the I - V curves of nitrogen, helium, argon, and ammonia, particularly for $V \leq 7$ V. We therefore believe that $V \leq 7$ V is consistent with the supply-limited regime where the effective field is already very high that all the molecules into the ionization zone are ionized and the current mildly increases with field. The supply-limited field-ion current does not depend on U_i , while it is a weak function of α , is proportional to the residing gas pressure, P_g , and is given by

$$I_{SL} = 2\pi r_w^2 e \frac{P_g}{(2\pi m k T)^{1/2}} \left(\frac{\pi \alpha E^2}{2kT} \right)^{1/2}, \quad (4)$$

where m is the molecular mass, and $kT \approx 26$ meV at room temperature. The amount of gas supplied into the gap does not follow the chamber pressure, especially at high pressures where D is small. As a result, the supply-limited field-ion currents of Figure 6b are not necessarily proportional to the equilibrium gas pressure inside the chamber. Note that For $V \lesssim 38$ V the curves tend to converge as the conduction becomes space charge limited (SCL). In this regime, the SCL *insulator injected plasma cube law* holds valid since the curves exhibit a slope of $S = 3$, i.e. $I \propto V^3$.

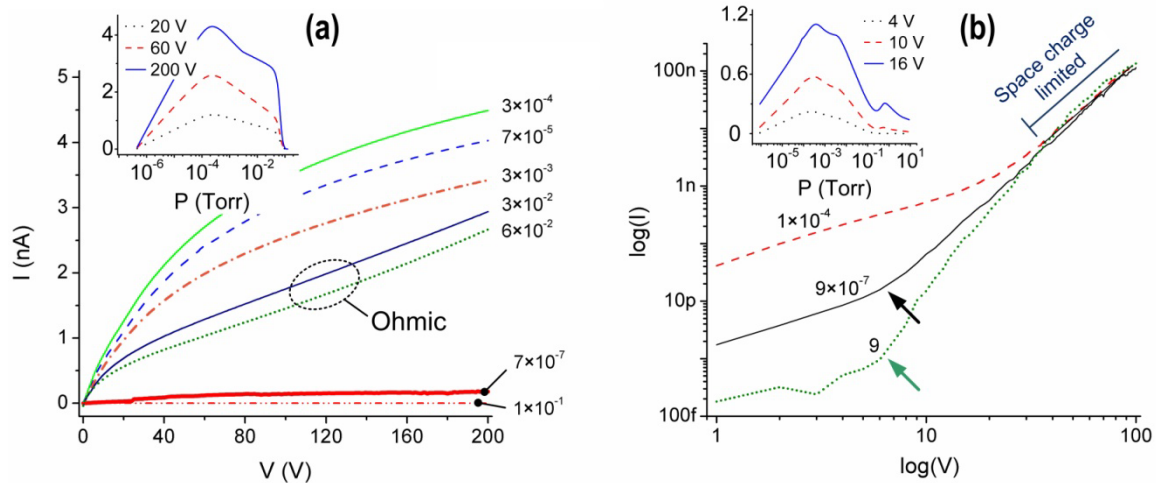


Figure 6. Current-Voltage curves of (a) IC.smooth, and (b) IC.branched#2 recorded in nitrogen within a wide pressure range. The insets show the dependence of the discharge currents on pressure at three bias voltages.

Much higher fields are required to ionize gas species adsorbed on the surface of the branches than those impinging on it. Ionization of an adsorbed particle is referred to as field desorption. The steep current rise observed at $V \approx 7$ V can be associated with desorption of field-adsorbed molecules along the nanowires which due to polarization forces crawl up to the apex of branches where the field is maximum. Depending on whether the ad-particle has covalent or ionic binding to the surface, the mechanism consists of field ionization preceded by complete or partial desorption in the former and direct ionic evaporation in the latter case¹⁷. Figures 7a-c show the I - V curves corresponding to field desorption of nitrogen, helium, and argon, measured using IC.branched#2 in three different pressures ($P = 0.1, 2$, and 10 Torr). In comparison to the low pressure scenario, at these high pressures, the rate of field ionization of the desorbing particle decreases due to two possible reasons: 1) formation of a multilayer of gas molecules on the emitter surface, and 2) reduction of the amount of gas accommodated in the gap as diffusivity shrinks with pressure. As a result, contrary to the low pressure case, where all the species in the gap are ionized ($P = 9 \times 10^{-7}$ and $P = 10^{-4}$ Torr in Figure 6b), the discharge current becomes a stronger function of U_j . The phenomenon is discernable in the I - V curves plotted in Figures 7a-c, as in general, the species with higher U_j have exhibited lower currents. Apparently, this can enable selective gas discrimination based on the field-ion I - V behavior of different gas types. These curves are the results of measurements carried in two consecutive days, that is, the curves of nitrogen (dash-dotted line) and helium (solid line) were obtained on the first day, and argon (short-dotted line), and again helium (dashed line) on the next. It is clearly seen that helium has generated a smaller field-ion current than nitrogen. In addition, activation and deactivation of adsorption sites with different bonding energies has produced kinks that are interestingly repeated in different gas types. The peaks correspond to the voltages at which these sites start to lose the adsorbed particles due to field desorption, therefore, the current ceases to rise until a site with a higher bonding energy is activated (valleys). Because of its higher U_j , the kinks corresponding to the field-ion current of helium lag in voltage as compared to those of nitrogen in Figures 7a-b, and to those of argon in Figure 7c. The fact that currents are pressure independent confirms that the ion current is initiated from adsorbed molecules rather than free molecules in the gap.

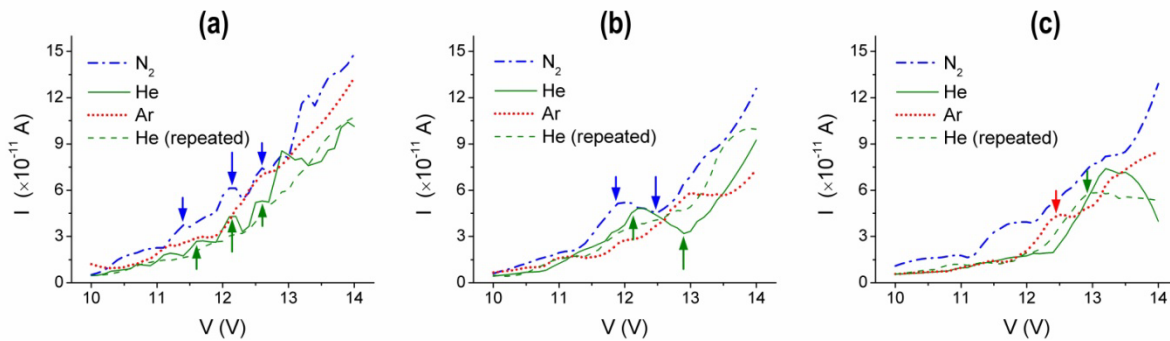


Figure 7. Field desorption I - V curves of nitrogen, helium, and argon at (a) $P = 0.1$, (b) $P = 2$, and (c) $P = 10$ Torr measured using IC.**branched#2**. The relative amplitudes of currents indirectly match the relative ionization potentials of the species, as helium with the highest U_I displays the lowest current. The arrows indicate voltages at which desorption sites with similar bounding energies are activated in the process of desorption of nitrogen and helium in cases (a) and (b), and desorption of argon and helium in (c).

Here we have measured anomalously strong field-ionization/desorption on gold catalyzed branching silicon nanowires. Such a phenomenon can be explained based on combination effects of geometrical field enhancement, silicon surface states close to the gold-silicon interface at the apex of the branches, and band gap widening due to quantum confinement in ultra-thin branches. Positive field penetration into the semiconductor causes upward band bending at the surface. The effective surface workfunction of the nanowire tip, ϕ_{eff} , increases by the amount of band bending, ϕ_s , causing $|U_I - \phi_{eff}|$ to decrease. As a result, the probability of electron tunneling into either the empty states of the degenerate levels above the Fermi level, or the surface states, increases as compared to metallic specimens¹⁰. In addition, field ionization on metal catalyzed silicon nano-branches appears to occur at a larger critical distance which explains the low currents measured herein. While unintentional incorporation of impurities in nanowires from the catalysts adversely affect the electrical properties of high performance electronic and photonic devices, the application of branching nanowires grown by VLS processes offer a unique advantage for ionization applications by using nanostructures with unmatched dimensions that readily come with high density of surface states associated with the impurities, and dangling bonds.

ACKNOWLEDGMENTS

This work was partially supported by the Natural Sciences and Engineering Research Council (NSERC) of Canada, a UC Davis research grant, an Army Research Office (ARO) research grant #55176-EL-DRP, and a grant sponsored by Hewlett-Packard Labs.

REFERENCES

- [1] Garnett, E. C., Tseng, Y.-C., Khanal, D. R., Wu, J., Bokor, J., and Yang, P., "Dopant profiling and surface analysis of silicon nanowires using capacitance-voltage measurements," *Nature Nanotechnology* 4, 311-314 (2009).
- [2] Salem, B., Dhalluin, F., Baron, T., Jamgotchian, H., Bedu, F., Dallaporta, H., Gentile, P., Pauc, N., den Hertog, M. I., Rouviere, J. L., and Ferret, P., "Chemical-vapour-deposition growth and electrical characterization of intrinsic silicon nanowires," *Materials Science and Engineering: B* 159-160, 83-86 (2009).

- [3] Volker, S., Joerg, V. W., Stephan, S., and Ulrich, G., "Silicon Nanowires: A Review on Aspects of their Growth and their Electrical Properties," *Advanced Materials* 21, 2681-2702 (2009).
- [4] He, R., and Yang, P., "Giant piezoresistance effect in silicon nanowires," *Nature Nanotechnology* 1, 42-46 (2006).
- [5] Wang, D., Qian, F., Yang, C., Zhong, Z., and Lieber, C. M., "Rational Growth of Branched and Hyperbranched Nanowire Structures," *Nano Letters* 4, 871-874 (2004).
- [6] Doerk, G. S., Ferralis, N., Carraro, C., and Maboudian, R., "Growth of branching Si nanowires seeded by Au-Si surface migration," *J. Mater. Chem.* 18, 5376-5381 (2008).
- [7] Bierman, M. J., and Jin, S., "Potential applications of hierarchical branching nanowires in solar energy conversion," *Energy & Environmental Science* 2, 1050-1059, (2009).
- [8] Modi, A., Koratkar, N., Lass, E., Wei, B., and Ajayan, P. M., "Miniaturized gas ionization sensors using carbon nanotubes," *Nature* 424, 171-174 (2003).
- [9] Banan-Sadeghian, R., and Kahrizi, M., "A novel miniature gas ionization sensor based on freestanding gold nanowires," *Sensors and Actuators A: Physical* 137, 248-255 (2007).
- [10] Miller, M. K., Cerezo, A., Hetherington, M. G., and Smith, G. D. W., [Atom Probe Field Ion Microscopy], Oxford, New York, (1996).
- [11] Ernst, L., and Block, J. H., "Field ion microscopy of germanium: Field ionization and surface states," *Surface Science* 49, 293-309 (1975).
- [12] Ohno, Y., Nakamura, S., Adachi, T., and Kuroda, T., "Field-ion microscopy of GaAs and GaP," *Surface Science* 69, 521-532 (1977).
- [13] Tsong, T. T., "Field penetration and band bending near semiconductor surfaces in high electric fields," *Surface Science* 81, 28-42 (1979).
- [14] Tsong, T. T., "Field penetration and band bending for semiconductor of simple geometries in high electric fields," *Surface Science* 85, 1-18 (1979).
- [15] Ernst, L., "On the field penetration into semiconductors in the field ion microscope," *Surface Science* 85, 302-308 (1979).
- [16] Gomer, R., [Field emission and field ionization], Harvard University Press, Cambridge, (1961).
- [17] Gomer, R., "Field Desorption," *J. Chem. Phys.* 31, 341-345 (1959).